Rapidity Dependence of HBT Radii Based on a Hydrodynamical Model

Kenji Morita[1]*

[1] *Department of Physics, Waseda University, Tokyo 169-8555, Japan*

We calculate two-pion correlation functions at finite rapidities based on a hydrodynamical model which does not assume explicit boost invariance along the collision axis. Extracting the HBT radii through χ^2 fits in both Cartesian and Yano-Koonin-Podgoretskiĭ parametrizations, we compare them with experimental results from the PHOBOS collaboration. Based on the results, we discuss longitudinal expansion dynamics.

Keywords: Hydrodynamical model; Pion interferometry; Boost invariance

I. INTRODUCTION

"Perfect fluidity" of the matter created at the Relativistic Heavy Ion Collider (RHIC) at BNL is some of the most exciting news in the field of high energy nuclear physics [1]. Experimental results and their comparison with theoretical calculation reveal that the matter created in Au+Au collisions should be something like a liquid of quarks and gluons, unlike a gas of almost free partons as naively expected [2]. One strong piece of evidence for this finding is the observation of large elliptic flow (v_2) and its agreement with a perfect fluid-dynamical calculation [3]. In order to reproduce the experimental result with such models, an equation of state assuming a partonic state at high temperature and a phase transition and rapid thermalization time ($\tau_0 \leq 1 \mathrm{fm}/c$) are required [3]. The hydrodynamic model based on numerical solutions of the relativistic hydrodynamic equation for perfect fluid has become an indispensable tool for theoretical analyses of relativistic heavy ion collisions. Furthermore, the model itself has been becoming more sophisticated in order to reproduce new experimental data with higher statistics. Currently, the most sophisticated calculations model a full three-dimensional (solving hydrodynamic equation without any symmetry) hydrodynamic expansion followed by a hadronic cascade [4, 5]. These models can reproduce most soft hadronic observables. Especially, the simultaneous description of particle ratios, transverse momentum spectra and elliptic flow is possible with such hybrid models.

However, there are still some insufficient ingredients in the hydrodynamic analyses. First, we don't have reasonable initial condition derived from first principles. Recently, the Color Glass Condensate (CGC) has been proposed as a suitable initial condition for relativistic heavy ion collisions [6]. This picture has been examined as an initial condition for a hydrodynamic model in Ref. [7] and found to give a good description of some observables in the case of fully hydrodynamic description of the collision process. However, this initial condition fails if one takes hadronic dissipation into account [4]. This fact suggests there is still open space for a dissipative partonic phase, or improvement of the initial condition.

Second, the equation of state (EoS) of QCD matter has not yet been fully understood. Since one of the most important merit of using a hydrodynamic model is that it can be directly related to the EoS, detailed information on the EoS for all region of temperature and baryonic chemical potential is indispensable. As for RHIC energies, the net baryon number observed at midrapidity is small enough to neglect it [8]. Nevertheless, the EoS at finite baryonic chemical potential may play an important role in the forward rapidity region and in heavy ion collisions at lower energies. Because of the well-known difficulty of lattice QCD at finite baryonic chemical potential [9], lattice QCD calculations have not yet provided the complete solution. For vanishing baryonic chemical potential, the lattice equation of state clearly shows a different behavior from the free parton gas [10], and a lattice-inspired EoS has been implemented in hydrodynamic calculations [11].

At last, in spite of the success in most soft observables, results of the two-pion momentum intensity correlation from such hydrodynamical models do not yet agree with experimental data. According to the symmetry of the wave function of two identical bosons, the two-particle correlation function can be related to sizes of the source from which particles are emitted. This fact is known as Hanbury Brown-Twiss (HBT) effect. Because it concerns source sizes, which depend on momentum of particle pairs due to collective flow, the pion correlation function is a diagnostic tool for the space-time evolution of the matter. Since the disagreement was first found with a (2+1)-dimensional model with boost invariance along the collision axis [12], many extensions such as an explicit longitudinal expansion [13, 14], incorporating chemical freeze-out [14], chiral model EoS [15], an opaque source [16], fluctuating initial conditions and continuous freeze-out [17], have been examined. The discrepancy has been reduced, but the situation is still unsatisfactory. There are various possibilities for further improvements.

So far discussion on the HBT radii at the RHIC has been limited to midrapidity because of the acceptances of the two experiments, STAR and PHENIX. PHOBOS also has measured the two-pion correlation function. By virtue of the wider acceptance of the PHOBOS detector, measurements at non-zero rapidity windows has been performed, and the data are now available in Ref. [18]. For analyses of such data in terms of the Cartesian parameterization [19, 20], it should be noted that there exists an additional HBT radius called "out-long cross term" [21] which vanishes at midrapidity due to

*Present Address: Institute of Physics and Applied Physics, Yonsei University, Seoul 120-749, Korea

the symmetry. This radius contains information on the correlation between freeze-out points on the transverse plane and those on the longitudinal direction. Hence, it is expected that this quantity is sensitive to longitudinal expansion dynamics beyond the boost-invariant approximation. Similar considerations also hold for the Yano-Koonin-Podgoretskiĭ parametrization which has three radius parameters and one velocity parameter called YK velocity [22, 23]. The PHOBOS data also provide rapidity dependence of the YKP radii and YK velocity [18], which may impose a restriction on the longitudinal expansion dynamics. Indeed, the initial matter distribution as an input for hydrodynamic calculations has not yet been fixed. This is indicated by Hirano in Ref. [24], in which two different initial energy density distributions result in reasonable agreement with experimental data of pseudorapidity distribution of charged hadrons measured in 130*A* GeV Au+Au collisions at RHIC.

In this work, we employ two different initial energy density distributions for the hydrodynamic equations, as in Ref. [24]. We focus our discussion on central collisions. Both of them are tuned so that they reproduce the pseudorapidity distribution of charged hadrons measured in the most central events at 200*A* GeV Au+Au collisions. Then, we compare the space-time evolution and shape of the freeze-out hypersurface of the fluids and see how the difference in the initial condition is reflected onto them. We calculate the two-pion correlation function as the most promising experimental observable to see the difference. Extracting the HBT radii through Gaussian fits, we compare them with the experimental results and discuss the transverse momentum and rapidity dependence of the HBT radii. In the next section, we briefly review the hydrodynamical model used in this work. Initial conditions are given in Sec. III. In Sec. IV, we show numerical solutions of hydrodynamical equations for the initial conditions given in Sec. III. Results for the HBT radii as compared with the experimental data are given in Sec. V. Section VI is devoted to a summary.

II. HYDRODYNAMICAL MODEL

The basic equation of hydrodynamical models is the energy-momentum conservation law

$$\partial_\mu T^{\mu\nu} = 0, \tag{1}$$

where $T^{\mu\nu}$ is the energy-momentum tensor. For a perfect fluid,

$$T^{\mu\nu} = (\varepsilon + P)u^\mu u^\nu - Pg^{\mu\nu}, \tag{2}$$

where $g^{\mu\nu} = \text{diag}(+, -, -, -)$ and ε, P and u^μ are the energy density, pressure and the four velocities of the fluid, respectively. If one takes a conserved charge i such as baryon number and strangeness into account, the conservation law

$$\partial_\mu(n_i u^\mu) = 0 \tag{3}$$

is added. Providing an EoS $P = P(\varepsilon, n_i)$, one can solve these coupled equations numerically.

In this work, we consider the baryon number charge as a conserved charge and adopt an equation of state which exhibits a first order phase transition on the phase boundary in

the $T - \mu_B$ plane from the free massless partonic gas with three flavors to the free resonance gas which consists of hadrons except for hyperons up to 2 GeV/c^2 of mass with excluded volume correction[25]. See Ref.[26] for the detail. The critical temperature T_c at vanishing baryonic chemical potential is set to 160 MeV. This model is basically same as the one used in Refs. [13, 16].

Defining the z-axis as the collision axis, we use a cylindrical coordinate system (τ, η_s, r, ϕ) as follows;

$$t = \tau\cosh\eta_s, \tag{4}$$
$$z = \tau\sinh\eta_s, \tag{5}$$
$$r_x = r\cos\phi, \tag{6}$$
$$r_y = r\sin\phi. \tag{7}$$

Here, $\tau = \sqrt{t^2 - z^2}$ is the proper time and $\eta_s = 1/2\ln[(t+z)/(t-z)]$ is the space-time rapidity. Since we focus on central collisions, we assume an azimuthally symmetric system. Then, by virtue of $u_\mu u^\mu = 1$, the four velocities are given in terms of a longitudinal flow rapidity Y_L and a transverse flow rapidity Y_T as

$$u^\tau = \cosh(Y_L - \eta_s)\cosh Y_T, \tag{8}$$
$$u^{\eta_s} = \sinh(Y_L - \eta_s)\cosh Y_T, \tag{9}$$
$$u^r = \sinh Y_L. \tag{10}$$

To solve the equations numerically, we employed a method based on the Lagrangian hydrodynamics which traces flux of the current. The numerical procedure is described in Ref. [27]. For treatment of the first order phase transition, we introduce a fraction of the volume of the QGP phase to express the energy density and net baryon number density at the mixed phase [26]. In this algorithm, we explicitly solve the entropy and baryon number conservation law. We checked that these quantities are conserved throughout the numerical calculation within 1% accuracy for a time step $\delta\tau = 0.01$ fm/c, by choosing proper mesh sizes of η_s and r directions.

III. INITIAL CONDITIONS

Firstly, we choose an initial proper time as $\tau_0 = 1$ fm/c. Initial values for other variables are given on this hyperbola. Longitudinal flow rapidity is set to the Bjorken's scaling ansatz $Y_L = \eta_s$ [28]. Transverse flow is simply neglected at the initial proper time [29]. For the matter distributions, we assume that the energy and baryon number density are proportional to the number of binary collisions. Hence, for the Woods-Saxon profile of the nucleon density in nuclei,

$$\rho_W(r, z) = \frac{\rho_0}{e^{(\sqrt{r^2 + z^2} - R)/\xi} + 1}, \tag{11}$$

where $R = 1.12A^{1/3} - 0.86A^{-1/3}$ fm is the radius of the nuclear with mass number A, $\xi = 0.54$ fm is the surface diffuseness and ρ_0 is the normal nuclear matter density, the density of binary collisions at vanishing impact parameter is given by

$$n_{BC}(r) = \sigma_0 \left[\int_{-\infty}^{\infty} dz\,\rho_W(r, z)\right]^2, \tag{12}$$

with σ_0 being the total inelastic nucleon-nucleon cross section which is absorbed into the proportionality constant between n_{BC} and matter distributions.

Then, the energy density distribution is parameterized with a "flat+Gaussian" form,

$$\varepsilon(\tau_0, \eta_s, r) = \varepsilon_0 \exp\left[-\frac{(|\eta_s| - \eta_{s0})^2}{2\sigma_{\eta_s}^2}\theta(|\eta_s| - \eta_{s0})\right]\overline{n_{BC}}(r).$$
(13)

Here, $\overline{n_{BC}}(r)$ is the normalized density of binary collisions (12), ε_0 the maximum energy density, and η_{s0} and σ_{η_s} are parameters which determine the length of the flat region and width of the Gaussian part, respectively. Similarly, the net baryon number density distribution is parameterized as

$$n_B(\tau_0, \eta_s, r) = n_{B0}\left\{\exp\left[-\frac{(|\eta_s| - \eta_{sD})^2}{2\sigma_{sD}^2}\right]\theta(|\eta_s| - \eta_{s0})\right.$$
$$\left.+ \exp\left[-\frac{(\eta_{s0} - \eta_{sD})^2}{2\sigma_{sD}^2}\right]\theta(\eta_{s0} - |\eta_s|)\right\}\overline{n_{BC}}(r), \qquad (14)$$

where n_{B0} is the maximum net baryon number density and η_{sD} and σ_{sD} are the shape parameters as in Eq. (13).

To calculate final particle distribution, we use the Cooper-Frye prescription [30]. The pseudorapidity distribution for a particle species i is given by

$$\frac{dN_i}{d\eta} = \frac{d_i}{(2\pi)^2}\int_0^\infty dk_t \frac{k_t|\mathbf{k}|}{k^0}\int_\Sigma k \cdot d\sigma f(k \cdot u, T, \mu_B), \qquad (15)$$

where k^μ is the momentum of thermally produced particles i with d_i being the number of degrees of freedom, the pseudo-rapidity η defined by $\eta = 1/2\ln[(|\mathbf{k}| + k_z)/(|\mathbf{k}| - k_z)]$, and $f(k \cdot u, T, \mu_B)$ describing the the equilibrium distribution functions. We take into account not only directly produced particles but also resonance decay contributions. The freeze-out hypersurface Σ is defined by picking a constant temperature, $T = T_f = 140$ MeV. Here, we assume that thermal and chemical freeze-out occur simultaneously. Since experimental data of particle yields can be well described by the statistical model with high chemical freeze-out temperature close to T_c [31], we cannot reproduce the correct particle yields with this lower freeze-out temperature. However, in hydrodynamic analyses, k_t spectra are sensitive to the thermal freeze-out temperature, which affects the transverse expansion. In this calculation, we set the freeze-out temperature so that pion k_t spectrum is roughly reproduced in IC B and set the same freeze-out temperature for IC A and IC B. Note that the freeze-out temperature depends on the choice of the transverse profile of the initial matter distribution because a steeper pressure gradient yields larger transverse flow. For example, even $T_f \simeq 150 - 160$ MeV is possible with an initialization based on pQCD+saturation model [32]. Our value is only slightly different from Ref. [24], where the initial profile is very similar. In order to reproduce both the particle yields and the k_t spectra in dynamical regimes, one should introduce separate freeze-out temperatures [14, 33] or go to hybrid approach [4, 5, 34, 35]. In this work, however, our main argument will not be so affected by the description of the freeze-out because we focus on longitudinal expansion.

TABLE I: Parameters in initial matter distributions.

	ε_0 [GeV/fm³]	η_{s0}	$\sigma_{\eta s}$	n_{B0} [fm⁻³]	η_{sD}	σ_{sD}
IC.A	23.0	1.0	1.48	0.47	2.2	0.9
IC.B	20.5	3.0	0.33	0.55	2.2	0.75

In Table I, two sets of the initial parameters are listed. The corresponding initial energy density distributions, resultant pseudorapidity distributions and transverse momentum distributions are illustrated in Fig. 1, 2 and 3, respectively. We have chosen two initial conditions, both of which reproduce the experimental data of PHOBOS for the pseudo-rapidity distribution of charged hadrons [36], and of PHENIX for the transverse momentum distributions of π^-, K^- and $\bar{p}$ [37], and of BRAHMS for the rapidity distribution of net protons [38]. These two initial conditions are characterized by two parameters, η_{s0} and σ_{s0}. One has small η_{s0} and large σ_{s0}, which we denote initial condition A (IC.A). The other, which we represent IC.B, has the opposite feature; η_{s0} is large and σ_{s0} is small. The initial energy densities are both much larger than experimental estimations (~ 5 GeV/fm³) based on Bjorken's formula [2], but note that ε_0 in Table I is not an *average* energy density but *maximum* energy density, which strongly depends on the profile of initial matter distributions [39]. We calculated pseudorapidity distributions for not only these two initial conditions, but also for intermediate ones by varying η_{s0} from 1.0 to 3.0, and found that they can also reproduce the experimental data by adjusting other parameters appropriately. Perhaps the best fit will exist in the middle of this parameter range [40]. Here, we choose the extreme cases in order to see differences in the space-time evolution of the fluids originating from the difference in the initial conditions.

IV. SPACE-TIME EVOLUTION OF THE FLUIDS

Figures 4 and 5 show the space-time evolution of the temperature distributions and deviation from the scaling solution $Y_L = \eta_s$, as a function of η_s at $r = 0$ for various τ, respectively. From these figures, we find that the space-time evolution at forward rapidity is quite different between IC.A and IC.B in spite of the fact that both solutions give similar pseudorapidity distributions of hadrons. In IC.B, the sharp decrease of temperature, which is identical to steep pressure gradient at forward rapidity, causes rapid acceleration of the longitudinal flow at the edge of the fluid. On the other hand, in IC.A, pressure gradient is rather gradual. Hence, the resultant deviation from the scaling solution is smaller. However, because pressure gradients exist at smaller η_s in IC.A, such deviations take place at $\eta_s \simeq 1$ while the flow maintains the scaling solutions up to $\eta_s \simeq 2$ in IC.B. This fact explains the slightly larger ε_0 in IC.A since faster longitudinal expansion than the scaling expansion pushes entropy per unit rapidity to forward rapidity [13, 41].

Although Figs. 4 and 5 show that there exist differences between IC.A and IC.B in the space-time evolution, it is not triv-
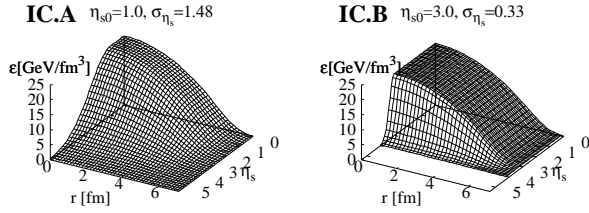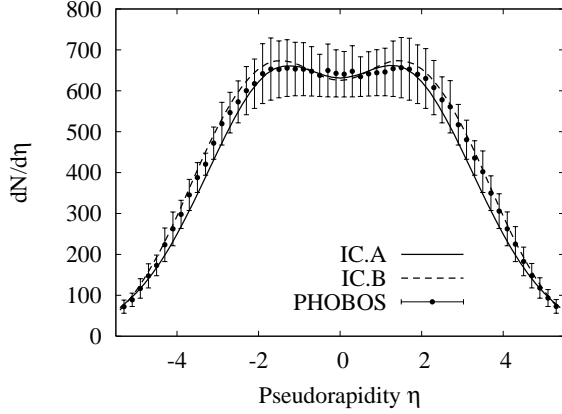
FIG. 1: Initial energy density distributions

FIG. 2: Pseudorapidity distribution. The solid line and dashed line stand for the initial conditions A and B, respectively. Experimental data measured by PHOBOS are taken from Ref.[36].
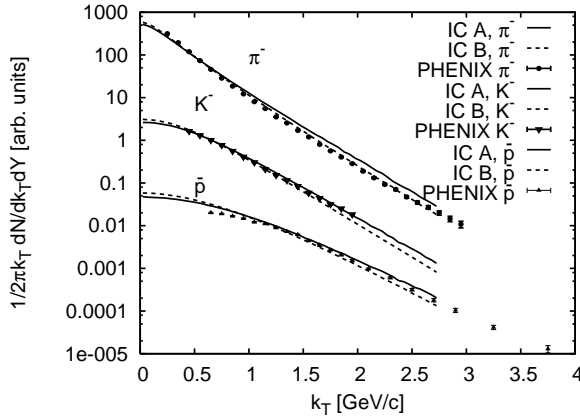

FIG. 3: Transverse momentum distribution of identified negatively charged hadrons. Spectra for kaons and anti-protons are scaled by factors 0.1 and 0.01 for a clear comparison of the slopes, respectively. Experimental data measured by PHENIX are taken from Ref. [37]. Identification of symbols is same as Fig. 2.
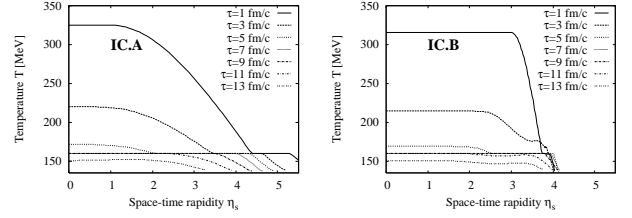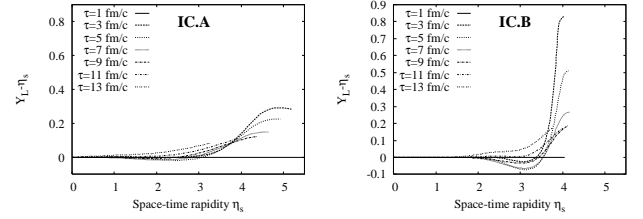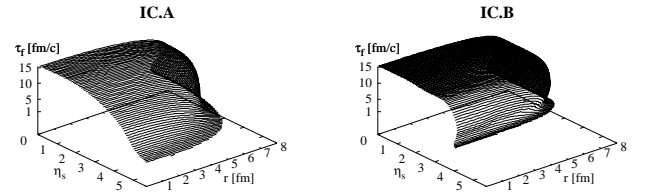

FIG. 4: Space-time evolution of temperature distributions at $r = 0$.

FIG. 5: Deviation from the scaling solution at $r = 0$.
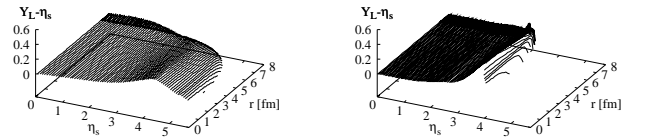

FIG. 6: Freeze-out hypersurface of the fluids.

FIG. 7: Deviation from the scaling solution on the freeze-out hypersurfaces.

ial that such differences can survive at the freeze-out hypersurfaces. Since hadrons strongly interact and provide information only at thermal freeze-out, differences in the freeze-out hypersurfaces are necessary to lead to a signature in hadronic experimental observables.

We show the freeze-out proper time τ_f of all fluid elements in Fig. 6. This characterizes the shape of the freeze-out hypersurface, which is expected to affect the HBT radii. In Fig. 6,

we can see that the system expands in the transverse direction in both of the fluids. Due to the same transverse profile, there is no apparent difference in the transverse direction. On the other hand, the shape of the hypersurface in the η_s direction shows some variations. In IC.B, expansion appears and the freeze-out proper time is mostly constant in the broad range of η_s, while it moderately decreases with η_s in IC.A. This is a consequence of the different longitudinal flow profile (Fig. 5). We also plot the deviation from the scaling solution at the freeze-out in Fig. 7. The large deviation seen at forward rapidity in IC.B (Fig. 5) survives until freeze-out. We will see

how these differences affect the HBT radii in the next section.

V. HBT RADII

A. Two-pion correlation function

Assuming that the source is completely chaotic, we can calculate the two-particle correlation momentum intensity correlation function through this formula [42]

$$C_2(q,K) = 1 + \frac{|I(q,K)|^2}{I(0,k_1)I(0,k_2)}, \tag{16}$$

where $q = k_1 - k_2$ is the four-relative momentum and $K = 1/2(k_1 + k_2)$ is the four-average momentum, with k_i being on-shell momentum of emitted pions. The interference term $I(q,K)$ can be chosen as

$$I(q,K) = \int_\Sigma K \cdot d\sigma\, e^{iq\cdot x} f(u \cdot K, T), \tag{17}$$

so that $I(0,k_i)$ reduces to the Cooper-Frye formula [43].

Experimentally, the two-pion correlation function is defined as

$$C_2(\mathbf{q}) = \frac{A(\mathbf{q})}{B(\mathbf{q})}, \tag{18}$$

where $A(\mathbf{q})$ is the measured two-pion pair distribution with momentum difference $\mathbf{q}$, and $B(\mathbf{q})$ is the background pair distribution generated from mixed events. Momentum acceptances are imposed separately in the numerator and the denominator. Accounting for the large acceptance in the PHOBOS experiment, $0.4 < Y_{\pi\pi} < 1.3$ for three K_T bins and $0.1 < K_T < 1.4$ GeV/c for three rapidity bins, we integrate the correlation function as follows:

$$C(q;K_T) = 1 + \frac{\int_{0.4}^{1.3} dY_{\pi\pi} |I(q,K)|^2}{\int_{0.4}^{1.3} dY_{\pi\pi} I(0,k_1)I(0,k_2)}, \tag{19}$$

$$C(q;Y_{\pi\pi}) = 1 + \frac{\int_{0.1}^{1.4} dK_T K_T |I(q,K)|^2}{\int_{0.1}^{1.4} dK_T K_T I(0,k_1)I(0,k_2)}. \tag{20}$$

For simplicity, we consider only directly emitted pions and neglect resonance decay contributions.

B. K_T dependence of the HBT radii in the Cartesian parametrization

Physical meaning of the HBT radii depends on the choice of three independent components of the relative momentum q. The most standard choice is the so-called Cartesian Bertch-Pratt parametrization [19, 20] $\mathbf{q} = (q_{out}, q_{side}, q_{long})$ in which "long" means parallel to the collision axis, "side" perpendicular to the transverse component of the average momentum $\mathbf{K_T}$ and "out" parallel to $\mathbf{K_T}$. In the case of azimuthally symmetric system as considered here, one can put $\mathbf{K_T} = (K_T, 0)$ so that $q_{out} = q_x$ and $q_{side} = q_y$. Note that $q_{long} = q_z$. Then, the

Gaussian form of the two-pion correlation function is given as [21]

$$C_{2\text{fit}}(\mathbf{q}) = 1 + \lambda \exp(-q_{out}^2 R_{out}^2 - q_{side}^2 R_{side}^2 - q_{long}^2 R_{long}^2 \\ - 2q_{out}q_{long}R_{ol}^2). \tag{21}$$

The HBT radii R_i can be extracted by a χ^2-fit to the above fitting function. For a chaotic source, the chaoticity parameter λ should become unity. However, the experimentally observed chaoticity is smaller than 1 because of such contributions as long-lived resonance decay [44]. Here we fix $\lambda = 1$ in the Gaussian fit to the calculated correlation functions with Eqs. (19) and (20).

By expanding the correlation function (16) for $q \cdot x \ll 1$, the size parameters R_i can be related to second order moments of the source function [21]. In the Cartesian parametrization, taking the longitudinal co-moving system (LCMS) makes the expression simple;

$$R_{out}^2 = \langle (\tilde{r}_x - \beta_\perp \tilde{t})^2 \rangle \\ = \langle \tilde{r}_x^2 \rangle - 2\beta_\perp \langle \tilde{r}_x \tilde{t} \rangle + \beta_\perp^2 \langle \tilde{t}^2 \rangle. \tag{22}$$

$$R_{side}^2 = \langle \tilde{r}_y^2 \rangle, \tag{23}$$

$$R_{long}^2 = \langle \tilde{z}^2 \rangle, \tag{24}$$

$$R_{ol}^2 = \langle (\tilde{r}_x - \beta_\perp \tilde{t})\tilde{z} \rangle, \tag{25}$$

where

$$\langle A(x) \rangle \equiv \frac{\int_\Sigma k \cdot d\sigma f(u \cdot k, T) A(x)}{\int_\Sigma k \cdot d\sigma f(u \cdot k, T)}, \tag{26}$$

$\tilde{x} \equiv x - \langle x \rangle$, and $\beta_\perp = k_T/E_{\mathbf{k}}$. Hence, R_{out}, R_{side} and R_{long} can be interpreted as a mixture of the thickness of the source and the emission duration, the transverse source size, and the longitudinal source size, as seen from the LCMS, respectively. The validity of these expressions for a hydrodynamical model is discussed in Ref. [45]. Although they have been shown to be good approximations, it is also pointed out that there are still some discrepancies, and one should use fitted HBT radii for comparison with the experimental data which are obtained from the fit [46].

Figure 8 shows results for the four HBT radii compared with the experimental data measured by PHOBOS [18]. For comparison of the initial conditions, any qualitative and quantitative difference cannot be seen in R_{out} and R_{side}, as expected from Fig. 6. R_{long} of IC.A is about 1 fm smaller than that of IC.B. This can be considered as a consequence of the fact that the deviation from the scaling solution at small η_s is larger in IC.A, because faster flow causes more thermal suppression of the emission region [13]. For these three radii, our calculation cannot reproduce the experimental results and show similar behavior with other perfect fluid dynamical calculations of Ref.[12–14, 16]. Especially R_{long} shows the largest deviation from experimental data, although the calculation is improved by including longitudinal expansion without explicit boost invariance [13, 14]. In the bottom of Fig. 8, the result of the out-long cross term is presented. Reflecting the uniform shape of the freeze-out hypersurface in Fig. 6, the value of R_{ol}^2
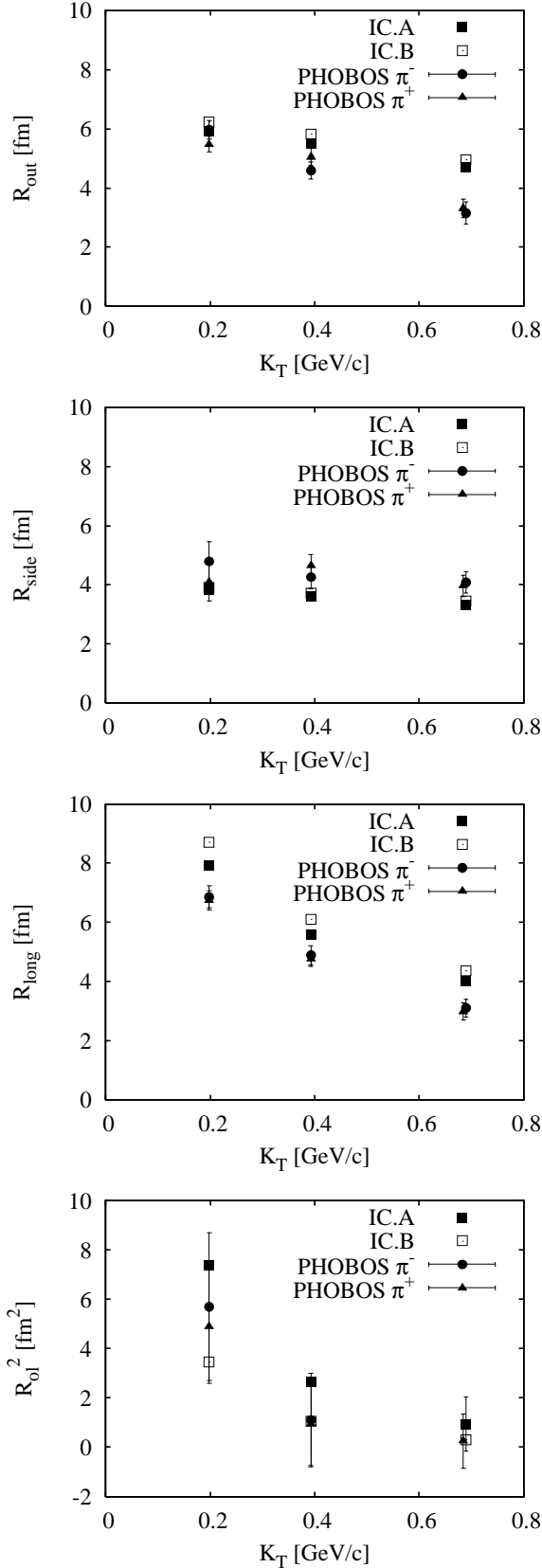
FIG. 8: K_T dependence of Cartesian HBT radii. Closed squares and open squares denote our results for IC.A and IC.B, respectively. Experimental data are taken from Ref. [18]. Error-bars for the experimental data are statistical only.

of IC.B is smaller than that of IC.A. At the lowest K_T bin, the difference is about 4 fm². Unfortunately, experimental uncertainty is still too large to distinguish which initial condition is favored. However, it should be noted that both of two results agree with the experimental data, in spite of the disagreement of other radii.

C. Rapidity dependence of the HBT radii in the YKP parametrization

In the YKP parametrization, three independent components of the relative momentum q are $q_\perp = \sqrt{q_x^2 + q_y^2}$, $q_\parallel = q_z = q_{\text{long}}$ and $q_\tau = E_1 - E_2$. Then, the Gaussian fitting correlation function is given as

$$C_{2\text{YKP}}(\mathbf{q}) = 1 + \lambda \exp\left[-R_\perp^2 q_\perp^2 - R_\parallel^2 (q_\parallel^2 - q_\tau^2) \right.$$
$$\left. - (R_\tau^2 + R_\parallel^2)(q \cdot U)^2 \right], \qquad (27)$$

where $U^\mu = \gamma(1, 0, 0, v_{\text{YK}})$, $\gamma = 1/\sqrt{1 - v_{\text{YK}}^2}$ and v_{YK} is the fourth fitting parameter called the YK velocity. The three HBT radii, $R_\perp$, $R_\parallel$ and R_τ are invariant under a longitudinal boost. Physical meaning of the parameters can be given in a similar manner [23] and becomes the simplest as follows, if one adopt the YK frame where $v_{\text{YK}} = 0$,

$$R_\perp^2 = \langle \tilde{r}_y^2 \rangle = R_{\text{side}}^2, \qquad (28)$$
$$R_\parallel^2 \simeq \langle \tilde{z}^2 \rangle = R_{\text{long}}^2, \qquad (29)$$
$$R_\tau^2 \simeq \langle \tilde{t}^2 \rangle. \qquad (30)$$

The main advantage of using YKP parametrization is that the three HBT radii directly give the transverse, longitudinal and temporal source size, that are seen from the YK frame. However, one should note that the latter two, (29) and (30), are approximate expressions which hold only if the source is not opaque [45]. Hence, $R_\parallel$ and R_τ cannot be always regarded as the source sizes in the presence of strong transverse flow which makes the source highly opaque [16]. The general expression of v_{YK} is complicated one [23] but it can be regarded as a longitudinal flow velocity of the source measured in an observer's frame.

We plot results of HBT radii for the YKP parametrization in Fig. 9. Though PHOBOS measures only at small values of rapidity, we calculate the HBT radii for $Y_{\pi\pi} = 0.602, 0.877, 1.122, 1.5, 2.0, 2.5, 3.0, 3.5$ and 4.0 and show the results as a prediction. For comparison between IC.A and IC.B, $R_\perp$ seems to barely reflect the uniform structure along η_s direction in IC.B. While $R_\parallel$ shows a difference of order 1 fm at small rapidity coming from the deviation of the scaling solution as well as in the third panel of Fig. 8, R_τ shows little difference and agrees with experiment. Large experimental errors will be due to the known difficulty of the limited kinematic region in the YKP parameterization [47]. Because of the large K_T window of the data, it is difficult to estimate the geometrical opacity effect on R_τ. If we assume this effect is small,
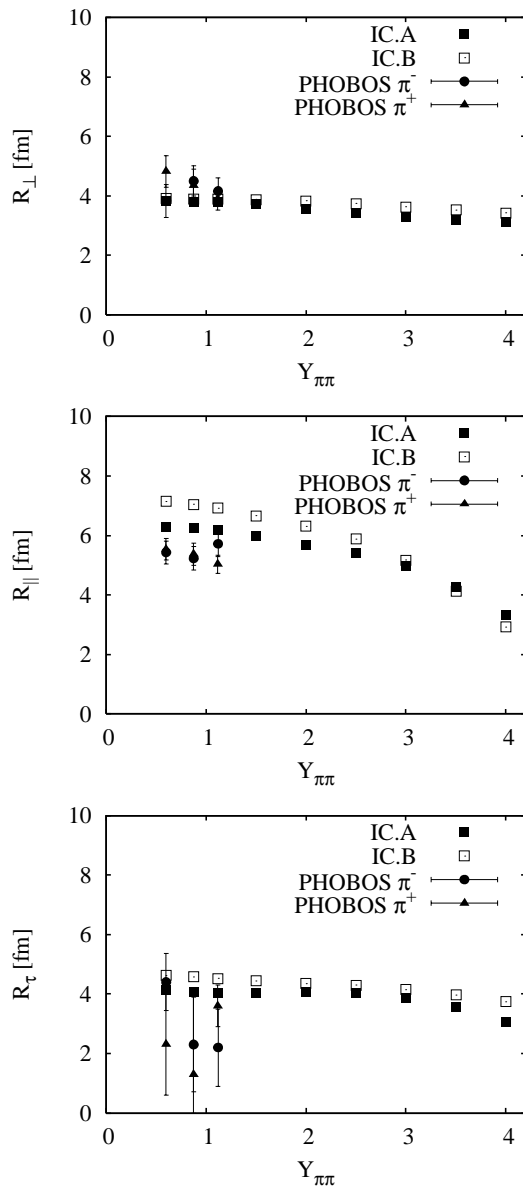
FIG. 9: HBT radii for the YKP parametrization. The identification of the symbols is the same as in Fig. 8.

a possible origin of the deviation of our result from the data is larger emission duration. Some model calculations based on source parametrization [48] and parametric exact solution of hydrodynamics [49] show very small emission duration time, 0-2 fm/c in agreement with data on the bottom panel of Fig. 9. We cannot see any significant differences in the HBT radii at forward rapidity expected from Figs. 6 and 7 which display the differences of the source shape and the longitudinal flow. This will come from the fact that the number of produced particles is larger at late freeze-out proper time in the case of the current freeze-out condition [45].

Finally, the Yano-Koonin rapidity $Y_{YK} = 1/2\ln[(1 + v_{YK})/(1 - v_{YK})]$ is shown as a function of $Y_{\pi\pi}$ in Fig. 10. Both results from IC.A and IC.B surprisingly agree with the exper-

imental data and show no difference between the two. In the forward rapidity region, our results show deviation from the infinite boost invariant case, which is indicated by the straight line. Although our solutions of longitudinal flow show deviation from the scaling solution (Figs. 5 and 7), the result would have to yield Y_{YK} larger than a given $Y_{\pi\pi}$, if Y_{YK} correctly represents the longitudinal source velocity. Hence, this deviation will be caused by the finite size effect [45] which becomes more significant at forward rapidity rather than the difference in the flow velocity.
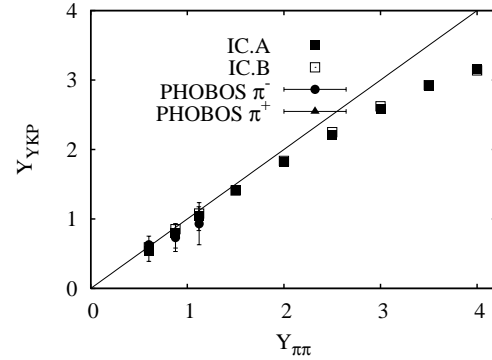

FIG. 10: The Yano-Koonin rapidity Y_{YK}. The identification of the symbols is the same as in Figs. 8 and 9. The solid line indicates the case of the infinite boost-invariant source.

VI. SUMMARY

In summary, we calculated the two-pion correlation function for two sources which are given by a hydrodynamical model without explicitly boost invariance along the collision axis. The two initial conditions are so chosen that both of them give consistent pseudorapidity distribution with the experimental data and have different shape in the longitudinal direction. Other model ingredient, initial transverse profile from the binary collision model, scaling solution for initial longitudinal flow, vanishing initial transverse flow, EoS with first order phase transition and Cooper-Frye freeze-out prescription with $T_f = 140$ MeV are the same in the two solutions. We find that there exist some differences in the space-time evolution of the fluids in spite of the fact that both fluids give similar particle distribution. The HBT radii are extracted from the two-pion correlation functions and compared with the experiment. In the Cartesian parametrization, the out-long cross term which arises at nonzero rapidities shows a difference between two initial conditions and the good agreements with the experimental data. The correlation function is also analyzed with the YKP parametrization. We find a small difference between the two initial conditions in $R_\parallel$ which reflects deviation from the scaling solution in the longitudinal expansion as well as R_{long} in the Cartesian parametrization. Possible sources of this disagreement are followings: EoS of current use exhibits first order phase transtion which makes the lifetime of the fluid longer, and assumes hadronic states is in fully chemical equilibrium. It is known that both crossover EoS [15] and incorporating chemical freeze-out [14] improve the lifetime

then R_{long} and $R_{\parallel}$. We used the conventional Cooper-Frye prescription for the freeze-out. Improvement of the freeze-out prescription by continuous freeze-out [11] and hybrid approach [4, 5] can yield larger R_{side} but this may lead to larger R_{out} because of extended emission duration. Nevertheless, as a transport calculation [50] shows, positive $x - t$ correlation in the source function may resolve this problem. Finally, in spite of the disagreement of the HBT radii, the YK rapidity shows a good agreement with the experimental data. Our calculation predicts some deviations at larger rapidities from the infinite boost-invariant case. Hence, measurements at this region is

needed for further understanding of the expansion dynamics.

[1] http://www.bnl.gov/bnlweb/pubaf/pr/PR _display.asp?prID=05-38

[2] I. Arsene *et al.*, (BRAHMS Collaboration), Nucl. Phys. A **757**, 1 (2005); B. B. Back *et al.*, (PHOBOS Collaboration), *ibid*, A **757**, 28 (2005); J. Adams *et al.*, (STAR Collaboration), *ibid*, A **757**, 102 (2005); K. Adcox *et al.*, (PHENIX Collaboration), *ibid*, A **757**, 184 (2005).

[3] P. F. Kolb, P. Huovinen, U. Heinz, and H. Heiselberg, Phys. Lett. B **500**, 232 (2001).

[4] T. Hirano, U. Heinz, D. Kharzeev, R. Lacey, and Y. Nara, Phys. Lett. B **636**, 299 (2006).

[5] C. Nonaka, S. A. Bass, arXiv:nucl-th/0607018.

[6] E. Iancu, R. Venugopalan, in *Quark-Gluon Plasma 3*, edited by R. C. Hwa, X. N. Wang, World Scientific, Singapore, 2004.

[7] T. Hirano and Y. Nara, Nucl. Phys. A **743**, 305 (2004).

[8] I. G. Bearden *et al.*, (BRAHMS Collaboration), Phys. Rev. Lett. **93**, 102301 (2004).

[9] For a review, S. Muroya, A. Nakamura, C. Nonaka, and T. Takaishi, Prog. Theor. Phys. **110**, 615 (2003).

[10] Y. Aoki, Z. Fodor, S. D. Katz, and K. K. Szabo, JHEP **0601**, 089 (2006).

[11] Y. Hama, R. P. G. Andrade, F. Grassi, O. Socolowski Jr., T. Kodama, B. Tavares, and S. S. Padula, Nucl. Phys. A **774**, 169 (2006).

[12] U. Heinz, P. Kolb, Nucl. Phys. A **702**, 269 (2002).

[13] T. Hirano, K. Morita, S. Muroya, and C. Nonaka, Phys. Rev. C **65**, 061902(R) (2002); K. Morita, S. Muroya, C. Nonaka, and T. Hirano, *ibid.*, **66**, 054904 (2002).

[14] T. Hirano, K. Tsuda, Phys. Rev. C **66**, 054905 (2002).

[15] D. Zschiesche, H. Stöcker, W. Greiner, and S. Schramm, Phys. Rev. C **65**, 064902 (2002).

[16] K. Morita, S. Muroya, Prog. Theor. Phys. **111**, 93 (2004).

[17] O. Socorowski,Jr., F. Grassi, Y. Hama, and T. Kodama, Phys. Rev. Lett. **93**, 182301 (2004).

[18] B. B. Back *et al.*, (PHOBOS Collaboration), Phys. Rev. C **73**, 031901(R) (2006).

[19] G. Bertsch, M. Gong, and M. Tohyama, Phys. Rev. C **37**, 1896 (1988).

[20] S. Pratt, T. Csörgő, and J. Zimányi, Phys. Rev. C **42**, 2646 (1990).

[21] S. Chapman, P. Scotto, and U. Heinz, Phys. Rev. Lett. **74**, 4400 (1995).

[22] F. Yano, S. Koonin, Phys. Lett. B **78**, 556 (1978); M. I. Podgoretskiǐ, Sov. J. Nucl. Phys. **37**, 272 (1983).

[23] Y. -F. Wu, U. Heinz, B. Tomášik, and U. A. Wiedemann, Eur. Phys. J. C **1**, 599 (1998).

[24] T. Hirano, Phys. Rev. C **65**, 011901(R) (2001).

[25] Note that, however, this EoS does not agree with recent lattice

QCD calculations which exhibit cross-over transition at vanishing and small μ_B [10].

[26] C. Nonaka, E. Honda, and S. Muroya, Eur. Phys. J. C **17**, 663 (2000).

[27] T. Ishii, S. Muroya, Phys. Rev. D **46**, 5156 (1992).

[28] J. D. Bjorken, Phys. Rev. D **27**, 140 (1983).

[29] Note that the existence of the initial transverse flow can improve results for transverse momentum spectra but is an open issue. In this work, however, we simply neglect it in order to avoid to add additional parameters such as flow strength and profile. Since we are mainly focusing on longitudinal expansion dynamics in this paper, this simplification will not affect our main argument.

[30] F. Cooper and G. Frye, Phys. Rev. D **10**, 186 (1974).

[31] P. Braun-Munzinger, D. Magestro, K. Redlich, and J. Stachel, Phys. Lett. B **518**, 41 (2001).

[32] K. J. Eskola, H. Niemi, P. V. Ruuskanen, and S. S. Räsänen, Phys. Lett. B **566**, 187 (2003).

[33] P. F. Kolb, R. Rapp, Phys. Rev. C **67**, 044903 (2003).

[34] S. A. Bass, A. Dumitru, Phys. Rev. C **61**, 064909 (2000).

[35] D. Teaney, J. Lauret, and E. V. Shuryak, Phys. Rev. Lett. **86**, 4783 (2003).

[36] B. B. Back *et al.*, (PHOBOS Collaboration), Phys. Rev. Lett. **91**, 052303 (2003).

[37] S. S. Adler *et al.*, (PHENIX Collaboration), Phys. Rev. C **69**, 034909 (2004).

[38] I. G. Bearden *et al.*, Phys. Rev. Lett. **93**, 102301 (2004).

[39] P. F. Kolb, U. Heinz, P. Huovinen, K. J. Eskola, and K. Tuominen, Nucl. Phys. A **696**, 197 (2001).

[40] L. M. Satarov, A. V. Merdeev, I. N. Mishustin, and H. Stöcker, arXiv:hep-ph/0606074 .

[41] K. J. Eskola, K. Kajantie, and P. V. Ruuskanen, Eur. Phys. J. C **1**, 627 (1998).

[42] E. V. Shuryak, Phys. Lett. B **44**, 387 (1973).

[43] S. Chapman, U. Heinz, Phys. Lett. B **340**, 250 (1994).

[44] K. Morita, S. Muroya, and H. Nakamura, Prog. Theor. Phys. **114**, 583 (2005); *ibid*, **116**, 329 (2006). See also references therein.

[45] K. Morita, S. Muroya, H. Nakamura, and C. Nonaka, Phys. Rev. C. **61**, 034904 (2000).

[46] E. Frodermann, U. Heinz, and M. A. Lisa, Phys. Rev. C **73**, 044908 (2006).

[47] B. Tomášik and U. Heinz, Acta. Phys. Slov. **49**, 251 (1999).

[48] F. Retiere, M. A. Lisa, Phys. Rev. C **70**, 044907 (2004).

[49] M. Csanád, T. Csörgő, and B. Lörstad, Nucl. Phys. A **742**, 80 (2004).

[50] Z. W. Lin, C. M. Ko, and S. Pal, Phys. Rev. Lett. **89**, 152301 (2002).